

INTERDISCIPLINARY  
MATHEMATICS  
INSTITUTE

2014:08

A 3D Hydrodynamic Model for  
Cytokinesis of Eukaryotic Cells

Jia Zhao and Qi Wang

IMI

PREPRINT SERIES

COLLEGE OF ARTS AND SCIENCES  
UNIVERSITY OF SOUTH CAROLINA

# A 3D Hydrodynamic Model for Cytokinesis of Eukaryotic Cells

Jia Zhao <sup>\*</sup>and Qi Wang <sup>†</sup>

## Abstract

In the late stage of the mitotic cycle of eukaryotic cells, cytokinesis ensues where a parent cell replicates its nucleus with the necessary genetical substances (i.e., DNAs and chromosomes) and splits into two similar offspring cells. This mitotic process involves complex chemical, biophysical and mechanical processes whose details are just begin to be unfolded experimentally. In this paper, we propose a full 3-D hydrodynamical model using a phase field approach to study the cellular morphological change during cytokinesis. In this model, the force along the contracting ring or cytokinetic ring, induced by remodeling of actin-myosin filament on cell cortex layer at a division plane of the parent cell during cytokinesis, is approximated using a proxy force anchored on the newly formed nuclei. The symmetric or asymmetric cell division, i.e. a parent cell dividing its cytoplasm to produce two equal sized or unequal sized offspring cells, is simulated numerically with the model. Our numerical results show that the location of the division plane and the contracting force along the cytokinetic ring on the division plane is essential for the cell division. In addition, our numerical study also shows that, during cytokinesis, surface tension of the cell membrane also contributes to this process by retaining the morphological integrity of the offspring cells. This model and the accompanying numerical simulation tool provides a solid framework to build upon with more sophisticated whole cell models to probe the cell mitotic process.

## 1 Introduction

Cell is the fundamental unit in all living organisms since animals and plants are all made up of cells of different varieties. The study of cells is therefore an essential part of research in biological science and medicine. Among many functions of a cell, one important function is the cell's ability to reproduce, which is also known as cell proliferation. Because of cell proliferation, all living organisms can grow and acquire their life. Given its unique role played in biological systems, cell study has been the focal point of biology for centuries. With the

---

<sup>\*</sup>zhao62@mailbox.sc.edu, Department of Mathematics, University of South Carolina, Columbia, SC, 29208, U. S. A.

<sup>†</sup>qwang@math.sc.edu, Tel/Fax: 803-777-6268/803-777-3783, Department of Mathematics and NanoCenter at USC, University of South Carolina, Columbia, SC 29028, USA; School of Mathematics, Nankai University, Tianjin, P. R. China, 300071; Beijing Computational Science Research Center, Beijing, P. R. China, 100084

advancement of experimental technologies today, more cell functions and micro-structures that endow the functions have been uncovered, which reveal an amazingly complex cosmo on its own.

One fundamental part in cell study is the cell reproductive cycle, where a parent cell undergoes a sequence of intercellular transformations and eventually divides into two or more offspring cells. For prokaryotic cells, the cell proliferation process is called binary division or binary fission, which is the primary method for reproduction. For eukaryotic cells, it's called cell mitotic process or mitosis. At the late stage of the cell mitotic process for eukaryotic cells, after the nucleus has been divided and chromosomes separated, the cell division process is also called cytokinesis. For eukaryotic cells, cell division is a much more complicated process than the division of prokaryotic cells. Despite of extensive studies on cells over the years, lots of important mechanisms in living cells still remain mysteries. A lot more need to be discovered experimentally as well as theoretically in order for one to fully understand how a tiny cell really works. It's commonly agreed upon that cell division is not simply driven by a single mechanism, but rather many factors which are intertwined. As one of the most spectacular part of the cell cycle, any single step goes wrong may lead to a catastrophe or failure, which may lead to an unwelcome outcome for instance cancer. Thus, a detailed understanding on cytokinesis can be of great benefits for understanding many diseases. For more details, readers are referred to the insightful review article on this topic in [27]. Readers can also find comprehensive review materials for animal cytokinesis in [7, 12] and for cytokinesis of bacteria in [8]. Besides, some works related to mechanical properties of cells during cytokinesis such as material properties of cells and sources of stresses can be found in [21, 25]. The study published in [9] discusses the molecular requirements for cytokinesis and the work in [2] addresses some recent advances in the mechanism of cytokinesis in animal, yeast and plant cells.

Experimental observations have provide us with a basic picture of cell mitosis. For eukaryotic cells, at the beginning of the cell mitotic process, the parent cell first duplicates its genetic substances and then forms a mitotic spindle consisting of microtubules [20]. Through a cascade of signaling processes [22], the actin and myosin molecules would undergo a self-assembly process to remodel the cell cortical layer, a layer rich in actin-filaments located immediately adjacent to the cell membrane [18]. In sync with the elongation of the mitotic spindle, more actin and myosin molecules ascend to a ring like region in a plane roughly orthogonal to the axis of the mitotic spindle to form the cytokinetic ring or contractile ring. The plane is called the cleavage plane or division plane [5]. As more actomyosin molecules are accumulated along the cytokinetic ring, a contracting force is generated directed inward toward the axis of the spindle [18]. The contracting force pushes the membrane inward to create what is known as the cleavage furrow [25]. The localized activation of the small GTPase Rho family of proteins at the cell division plane controls the position of the contractile ring [28]. When Rho is specifically activated at the division plane within the cortex, it promotes actin polymerization and myosin-2 activation via Rho effector proteins. Rho-GTP promotes actin filament assembly and myosin-2 assembly [6]. The contractile ring is a dynamic structure, in which F-actin and myosin-2 are continuously assembled and disassembled to maintain a contracting force to squeeze the cell along the contractile ring. For eukaryotic cells, the positioning of contractile ring and cleavage furrow is regulated by distribution of long astral microtubules (MT) [24]. Besides, it has been shown that the cell geometry can

influence the position of the cell division plane [19] and ultimately affect the morphology of the offspring cells.

In addition to the vast amount of data from experimental observations, theorists have been trying to come up with testable hypothesis and models to decipher underlying mechanisms that control the cell division process. In [1], the author proposed a mathematical model for cell cleavage for the sea urchin by considering chemotactic motion of the centrosomes. In [23], the author developed a mechanical cell division model by a level-set approach, highlighting the furrow thinning trajectories. In [26], the author formulated an immersed boundary approach for modeling cell division focusing primarily on the mechanical aspect of cell division, which has been extended by [15] to study a single axisymmetric cell growth and division. The correlation between cell shape elongation and the orientation of the division axis has been studied in [29]. Besides, a model based on polymer dynamics to study spindle dynamics during cell division has been developed in [30].

Given the theoretical attempts made so far, there has been very little theoretical work done to resolve cytokinesis in full 3D using hydrodynamic models. Hence, in this paper, we set out to develop a 3D hydrodynamic model for cell division systematically by a phase field approach. Phase field methods have gained tremendous attention in last few decades, in particular, for the study of interfacial problems. The advantage of phase field methods, compared to the traditional sharp interface method, is that the interface is naturally incorporated in the model formation such that it does not need to be tracked separately. This reduces the computational cost tremendously. In the phase field formation, there is a parameter controlling the thickness of the interface. The phase field model converges to its sharp interface limit [4] as the thickness of the interface approaches zero. For cells, the *coarse-grained membrane and other interfaces within a cell* do not need to be very sharp, which makes the phase field formulation a good choice for describing the multiphasic structure in a cell.

Our objective in modeling cell division is to by develop a mathematical model systematically based on a phase field approach, where the cytoplasm, cell nucleus, and extra-cellular matrix are treated as three different multiphasic components of a complex fluid mixture. Given the complexity of a cell, a viable model must be built step by step by incorporating more complex mechanochemical details incrementally. The first important step is therefore to build a framework to simulate the morphological change of the cell membrane during cell division by highlighting the most dominant mechanism during the process. The most dominating factor that one has identified is the existence of the contractile ring within the cortex, which is primarily consisted of F-actins and myosins. Modeling the detail of the cortex remains our goal for this project. However, the effective force that squeezes the cell during cytokinesis is the contractile force exerted by the contractile ring. To highlight this mechanism in a simplistic way, we employ a proxy force in lieu of the contractile force generated by the actomyosin dynamics in the cortex in the model. We remain committed to develop the more detailed model for the cortical layer and the contractile ring within it, but defer it to a future paper. The governing system of equations in the model consists of the transport equation for each phase variable in the form of the volume fraction for that phase, continuity equation and the momentum balance equation. We discretize the governing partial differential equations and solve it using a finite difference method on a GPU in full 3D space and time. Numerical simulations, which will be discussed below, show several inspiring

morphologies during cell division that match well with the experimental observations.

The rest of the paper is organized into three sections. In section two, we present the multi-phase hydrodynamic model for the whole cell in a simplified picture. It is followed by a brief discuss on its numerical discretization and implementation issues. Finally, we present three numerical results and discuss their comparison with available experimental observations.

## 2 Mathematical Formulations of MutliPhase-field Models

In this section, we propose a mathematical model for the cell division process given in a phase field formulation. In this model, we treat the cell and the surrounding liquid environment as a fluid mixture in the form of a single fluid with multiple components. The volume fractions of cytoplasm, nucleus and the buffer fluid outside the cell are denoted by  $\phi_1, \phi_2$  and  $\phi_3$ , respectively. Here, we assume the buffer is a viscous fluid, so is the nucleus. The cytoplasm can be treated as a viscoelastic fluid. In this paper, we also treat it as a viscous fluid within the time scale of interest for simplicity.  $\eta_i, i = 1, 2, 3$  are used to represent the respective viscosities for the three phases, respectively. The cell membrane (together with the cortical layer) is the level set defined by  $\{\phi_1 = \frac{1}{2} = \phi_3\}$  and the membrane of the nucleus is the level set defined by  $\{\phi_2 = \frac{1}{2} = \phi_1\}$ . Notice that this is a globally multi-phase while locally binary system since there is no contact between nucleus and buffer at any time. The volume-average velocity and density for this fluid mixture is defined as

$$\mathbf{v} = \sum_{i=1}^3 \phi_i \mathbf{v}_i, \quad \rho = \sum_{i=1}^3 \phi_i \rho_i, \quad (1)$$

where  $\mathbf{v}_i, \rho_i$  is the effective velocity and density for component  $i, i = 1, 2, 3$ . For incompressible materials, we enforce

$$\phi_1 + \phi_2 + \phi_3 = 1. \quad (2)$$

### 2.1 Thermodynamic free energy

We denote the domain in which the cell resides together with the buffer fluid as  $\Omega$ . The free energy of this mixture system is proposed as follows,

$$F = \int_{\Omega} f d\mathbf{x}, \quad (3)$$

where  $f$  is the free energy density function. There are different choices for the free energy density function of the three phase fluid. Here we adopt a simple one:

$$f = \frac{1}{2} \left( \gamma_A \|\nabla \phi_1\|^2 + \gamma_B \|\nabla \phi_2\|^2 + \gamma_C \|\nabla \phi_3\|^2 + \gamma_1 \phi_1^2 \phi_2^2 + \gamma_2 \phi_2^2 \phi_3^2 + \gamma_3 \phi_3^2 \phi_1^2 + \gamma_{123} \phi_1^2 \phi_2^2 \phi_3^2 \right). \quad (4)$$

An alternative is given by

$$f = \frac{1}{2} \left( \gamma_A \|\nabla \phi_1\|^2 + \gamma_B \|\nabla \phi_2\|^2 + \gamma_C \|\nabla \phi_3\|^2 + \gamma_1 \phi_1^2 (1 - \phi_1)^2 + \gamma_2 \phi_2^2 (1 - \phi_2)^2 + \gamma_3 \phi_3^2 (1 - \phi_3)^2 + \gamma_{123} \phi_1^2 \phi_2^2 \phi_3^2 \right), \quad (5)$$

where  $\gamma_A, \gamma_B, \gamma_C$  govern the strength of the conformational entropy between different components,  $\gamma_1, \gamma_2, \gamma_3$  control the strength of the bulk/mixing energy for each pair of components, and  $\gamma_{123}$  is a Lagrangian multiplier to penalize the coexistence of the distinct phases. Our numerical studies show that these two choices of free energy density functions yield qualitatively the same results. Thus, in our study presented in this paper, we choose the second, i.e. equation (5). We remark that more features can be added to the model by augmenting the corresponding free energy.

## 2.2 Transport equations for biomass

Given the specific form of the free energy density (5), we assume that each component in the fluid mixture is convected by the volume-averaged velocity as well as transported via the osmotic pressure. Then, the transport equation for phase variables are given as follows

$$\partial_t \phi_i + \nabla \cdot (\mathbf{v} \phi_i) = \nabla \cdot \left( \sum_{j=1}^3 \alpha_{ij} \nabla \frac{\delta f}{\delta \phi_j} \right) + g_i, \quad i = 1, 2, 3, \quad (6)$$

where  $(\alpha_{ij})$  is the motility matrix and  $g_i$  are the reactive terms, respectively.

Note that the volume fractions add up to 1:  $\sum_{i=1}^3 \phi_i = 1$  for incompressible mixtures. This along with the Onsager reciprocal principle implies [16, 17]

$$\sum_{j=1}^3 \alpha_{ij} = 0, \quad \alpha_{ij} = \alpha_{ji}. \quad (7)$$

The off-diagonal motility coefficients can be obtained from the diagonal coefficients

$$\alpha_{12} = \frac{1}{2}(\alpha_{33} - \alpha_{11} - \alpha_{22}), \quad \alpha_{13} = \frac{1}{2}(\alpha_{22} - \alpha_{11} - \alpha_{33}), \quad \alpha_{23} = \frac{1}{2}(\alpha_{11} - \alpha_{22} - \alpha_{33}), \quad (8)$$

where we assume the diagonal motility parameters have the following form

$$\alpha_{ii} = \lambda_i \phi_i (1 - \phi_i), \quad (9)$$

with  $\lambda_i$  representing the strength of motility parameters for the corresponding component  $i$ ,  $i=1,2,3$ .

By incompressibility condition, it follows that

$$\sum_{i=1}^3 g_i = 0. \quad (10)$$

At the onset of cell division, the parent cell normally increases in cytoplasmic and organelle volume (the G1 phase) as well as increases in genetic materials (the G2 phase) right before

the replication during the S phase. This process can be modeled by proposing the reactive kinetics for the time rate of change in the volume fractions:

$$g_1 = c_1 H_1(t) \phi_1 \phi_3 - c_2 H_2(t) \phi_1 \phi_2, \quad (11)$$

$$g_2 = c_2 H_2(t) \phi_1 \phi_2, \quad (12)$$

$$g_3 = -c_1 H_1(t) \phi_1 \phi_3. \quad (13)$$

Here  $H_i(t)$ ,  $i = 1, 2$ , are Heviside functions defined by

$$H_1(t) = \begin{cases} 1, & t < t_1, \\ 0, & t \geq t_1, \end{cases} \quad H_2(t) = \begin{cases} 1, & t < t_2, \\ 0, & t \geq t_2, \end{cases} \quad (14)$$

where  $t_1$  is the critical checkpoint, at which the parent cell has just duplicated its volume,  $t_2$  is the critical checkpoint, at which the nucleus has doubled its volume. Thus, before  $t_1$  the parent cell keeps reproducing its cytoplasm to expand volume. After it doubles its volume, reproduction of cytoplasm ceases and cell proliferation begins. The growth kinetics is assumed to be originated from the interface between the buffer and cytoplasm as well as the nucleus and the cytoplasm.

We remark that this multi-phase field model is consistent, in term of reducing to the phase field model with less physical phases. First of all, when the component  $i$  is not present in the mixture at the initial time, the component will be absent from the system during the time evolution of the system, i.e. given  $i \in N$ ,

$$\phi_i(0) = 0 \rightarrow \phi_i(t) = 0, \forall t \geq 0. \quad (15)$$

Secondly, when there are only  $n < N$  phases in the model, the N-phase model naturally reduces to the n-phase model.

Although our formulation in equation (6) is consistent, in real numerical simulations, we don't need to calculate every single phase due to the incompressibility constraint. In our later discussion, we only keep track of the transport of  $\phi_2$  and  $\phi_3$ , since  $\phi_1$  can be obtained through the incompressibility condition (2).

## 2.3 Continuity and momentum equation

In order to close this system, we need to supplement the system with the continuity equation and momentum equation for the fluid mixture. By assuming the average velocity in the fluid mixture solenoidal, we have

$$\rho(\partial_t \mathbf{v} + \mathbf{v} \cdot \nabla \mathbf{v}) = -\nabla p + \nabla \cdot \tau + \mathbf{F}_e, \quad (16)$$

$$\nabla \cdot \mathbf{v} = 0, \quad (17)$$

where  $p$  is the hydrostatic pressure and  $\tau$  is the viscoelastic stress tensor and  $\mathbf{F}_e$  is the elastic body force yielding the surface tension of the cell membrane and the contractile force due to actin-myosin filaments. The viscoelastic stress tensor is proposed as follows,

$$\tau = 2 \sum_{i=1}^3 \eta_i \mathbf{D}_i + \tau_e, \quad (18)$$

where the first term sums up the viscous stress from each component, and the second term  $\tau_e$  is the elastic stress for the cytoplasm. A constitutive equation could be proposed for  $\tau_e$  relating to the specific structure of the cortex layer. In this paper, however, we set  $\tau_e = 0$  for the time scale of our interest and simplicity.

For the elastic body force or the interfacial force  $\mathbf{F}_e$ , we adopt the surface force yielded by the variation of the free energy. In addition, we propose a proxy force mimicing the cytokinetic ring, a contractible ring responsible for the cytokinesis of the animal cell, which is similar to the one used in [15],

$$\mathbf{F}_e = \sum_{j=1}^3 \frac{\delta F}{\delta \phi_j} \nabla \phi_j + \kappa_{\phi_1} f_{d1} \phi_1 \nabla \phi_1 + \kappa_{\phi_2} f_{d2} \phi_2 \nabla \phi_2, \quad (19)$$

where the first term is the interfacial force, due to the material change at the interface between each component and the second term is the proxy force mimicing the normal force generated by the cytokinetic ring, consisting of actomyoiso networks immediate within the cell membrane. We note, this proxy force provides the contractible force necessary for dividing the cell. As we alluded to in the introduction, we will leave the model of tracking the spatial distribution of actin-filament networks regulated by myosins in the cytokinetic ring for a future work. Specifically, we use  $\kappa$  to denote the mean curvature,

$$\kappa = -\nabla \cdot \mathbf{n}, \quad \mathbf{n} = -\frac{\nabla \phi}{|\nabla \phi|}. \quad (20)$$

In phase field formulation, it is approximated by

$$\kappa = \frac{1}{|\nabla \phi|} \left( \nabla^2 \phi - \frac{2}{\varepsilon} \phi(1 - \phi)(1 - 2\phi) \right), \quad (21)$$

where  $\varepsilon$  is the thickness of the interface, and  $f_{di}$ ,  $i=1,2$  denote the strength of the cytokinetic ring force, which by following the idea in [15] are proposed as follows

$$f_{d1} = H_{d1}(\phi_2, t) \frac{\gamma_{d1}}{||\mathbf{x} - c_1| - |\mathbf{x} - c_2|| + \varepsilon_d}, \quad f_{d2} = H_{d2}(\phi_3, t) \frac{\gamma_{d2}}{||\mathbf{x} - c_1| - |\mathbf{x} - c_2|| + \varepsilon_d}, \quad (22)$$

where

$$H_{d1}(\phi_2, t) = \begin{cases} 0, & \text{otherwise,} \\ 1, & \phi_2 = 0 \quad \& t > t_3. \end{cases} \quad H_{d2}(\phi_3, t) = \begin{cases} 0, & \text{otherwise,} \\ 1, & \phi_3 = 0 \quad \& t_2 < t < t_3. \end{cases} \quad (23)$$

are heaviside functions to restrict the force on cell membrane and the nucleus membrane at different stages of the cell division process, respectively, and  $c_1$  and  $c_2$  are the mass centers of the separated nuclei, respectively, i.e.,

$$c_1 = \frac{\int_{\Omega_1} \phi_2(\mathbf{x}) \mathbf{x} d\mathbf{x}}{\int_{\Omega_1} \phi_2(\mathbf{x}) d\mathbf{x}}, \quad c_2 = \frac{\int_{\Omega_2} \phi_2(\mathbf{x}) \mathbf{x} d\mathbf{x}}{\int_{\Omega_2} \phi_2(\mathbf{x}) d\mathbf{x}}$$

$\Omega_1$  and  $\Omega_2$  are the domains occupied by the two nuclei,  $\gamma_{di}$ ,  $i = 1, 2$  are two parameters characterizing the strength of  $f_{di}$ , respectively, and  $\varepsilon_d$  is a small number employed here to



avoid the singularity of  $f_{di}$ . Here,  $t_2$  is the checkpoint for the nucleus to begin separating after the size of the cell has been doubled and  $t_3$  is the critical checkpoint when the nucleus has been divided into two separate nuclei.

Notice that this cytokinetic ring force counters the force due to the one of surface tension along the cytokinetic ring. We did not incorporate this cytokinetic ring force into the thermodynamic free energy since this is a proxy for the active force generated by actin-myosin filament on the cytokinetic ring through the released of the hydrolyzed ATP. In the current context, it is not a potential force.

## 2.4 Dimensionless governing equations in the three phase model

We denote the reference time scale as  $t_0$ , reference length scale as  $h$  and reference mass density as  $\rho_0$ . Then, the variables and parameters are nondimensionalized as follows:

$$\begin{aligned}\tilde{\rho} &= \frac{\rho}{\rho_0}, \tilde{\mathbf{x}} = \frac{\mathbf{x}}{h}, \tilde{t} = \frac{t}{t_0}, \tilde{\mathbf{v}} = \frac{\mathbf{v}t_0}{h}, \tilde{\alpha}_{ij} = \frac{\alpha_{ij}}{t_0}, i, j = 1, 2, 3, \\ \tilde{\Gamma}_s &= \frac{\gamma_s k T t_0^2}{\rho h^4}, s = A, B, C, \tilde{\Gamma}_s = \frac{\gamma_s k T t_0^2}{\rho_0 h^2}, s = 1, 2, 3, 123, \quad Re_i = \frac{\rho_0 h^2}{\eta_i t_0}, i = 1, 2, 3.\end{aligned}\tag{24}$$

The governing equations in dimensionless form are summarized below.

$$\left\{ \begin{array}{l} \rho(\partial_t \mathbf{v} + \mathbf{v} \cdot \nabla \mathbf{v}) = \nabla \cdot (\sum_{i=1}^3 \eta_i \phi_i (\nabla \mathbf{v} + \nabla \mathbf{v}^T)) - \nabla p + \mathbf{F}_e, \\ \nabla \cdot \mathbf{v} = 0, \\ \partial_t \phi_i + \nabla \cdot (\mathbf{v} \phi_i) = \nabla \cdot (\sum_{j=1}^3 \alpha_{ij} \nabla \frac{\delta F}{\delta \phi_i}) + g_i, \quad i = 1, 2, 3, \end{array} \right.\tag{25}$$

where

$$\begin{aligned}g_1 &= c_1 H_1(t) \phi_1 \phi_3 - c_2 H_2(t) \phi_1 \phi_2, \\ g_2 &= c_2 H_2(t) \phi_1 \phi_2, \\ g_3 &= -c_1 H_1(t) \phi_1 \phi_3, \\ \mathbf{F}_e &= \sum_{j=1}^3 \frac{\delta F}{\delta \phi_j} \nabla \phi_j + \sum_{i=1}^2 \kappa_{\phi_i} f_{di} \phi_i \nabla \phi_i.\end{aligned}\tag{26}$$

This partial differential equation system will be discretized using a finite difference method.

## 3 Numerical methods

For these coupled PDEs, we use the extrapolation strategies to decouple them. That is, for each time step, we solve the momentum equation firstly using the extrapolated data for the biomass and functional components. Then with the updated velocity, we solve the transport equations for the volume fractions and the functional components one by one. We note that, in the following context, any variable with an overline  $(\bullet)^{n+1}$  represents a second-order extrapolation from  $n$  and  $n - 1$  steps.

For the momentum equation, we use the modified Gauge-Uzawa method [11] to calculate the average velocity. Recall that the momentum equation is given by

$$\rho\left(\frac{\partial \mathbf{v}}{\partial t} + \mathbf{v} \cdot \nabla \mathbf{v}\right) = \nabla \cdot \boldsymbol{\tau} - \nabla p + \mathbf{F}_e. \quad (27)$$

By adding a second order term  $-\frac{1}{Re_a}\nabla^2\mathbf{v}$  on both sides, where  $Re_a$  is the averaged Reynolds number, we rewrite the momentum equation into

$$\rho\left(\frac{\partial \mathbf{v}}{\partial t} + \mathbf{v} \cdot \nabla \mathbf{v}\right) - \frac{1}{Re_a}\nabla^2\mathbf{v} = -\nabla p + \mathbf{F}_e - \frac{1}{Re_a}\nabla^2\mathbf{v}. \quad (28)$$

The Gauge-Uzawa method is given by three steps listed below.

1. Prediction:

$$\left\{ \begin{array}{l} \rho^{n+1}\left[\frac{3\mathbf{u}^{n+1}-4\mathbf{v}^n+\mathbf{v}^{n-1}}{2\delta t}\right] + \rho^{n+1}\bar{\mathbf{v}}^{n+1} \cdot \nabla \bar{\mathbf{v}}^{n+1} + \frac{1}{2}(\nabla \cdot (\rho^{n+1}\bar{\mathbf{v}}^{n+1}))\bar{\mathbf{v}}^{n+1}, \\ + \frac{1}{Re_s}\nabla s^n + \nabla p^n - \frac{1}{Re_a}\nabla^2\mathbf{u}^{n+1} = \bar{\mathbf{R}}^{n+1} - \frac{1}{Re_a}\nabla^2\bar{\mathbf{v}}^{n+1-\varepsilon}, \\ \mathbf{u}^{n+1} \cdot \mathbf{n}|_{y=0,L_y} = 0, \end{array} \right. \quad (29)$$

2. Projection:

$$\left\{ \begin{array}{l} -\nabla \cdot \left(\frac{1}{\rho^{n+1}}\nabla\psi^{n+1}\right) = \nabla \cdot \mathbf{u}^{n+1}, \\ \frac{\partial\psi^{n+1}}{\partial n}|_{y=0,L_y} = 0, \end{array} \right. \quad (30)$$

3. Correction:

$$\left\{ \begin{array}{l} \mathbf{v}^{n+1} = \mathbf{u}^{n+1} + \frac{1}{\rho^{n+1}}\nabla\psi^{n+1}, \\ s^{n+1} = s^n - \nabla \cdot \mathbf{u}^{n+1}, \\ p^{n+1} = p^n - \frac{3\psi^{n+1}}{2\delta t} + \frac{1}{Re_a}s^{n+1}, \end{array} \right. \quad (31)$$

where

$$\bar{\mathbf{R}}^{n+1} = \frac{1}{2}\nabla \cdot \left( \left( \sum_{i=1}^3 \bar{\phi}_i^{n+1} \eta_i \right) (\nabla \bar{\mathbf{v}}^{n+1} + \nabla \bar{\mathbf{v}}^{T^{n+1}}) \right) + \sum_{i=1}^3 \bar{\mu}^{n+1} \nabla \bar{\phi}_i^{n+1} + \sum_{i=1}^2 \kappa_{\phi_i} f_{di} \bar{\phi}_i^{n+1} \nabla \bar{\phi}_i^{n+1}, \quad (32)$$

and  $\varepsilon = 0.05$ . The averaged Reynolds number  $Re_a$  is computed by

$$\frac{1}{Re_a} = \min\left(\frac{1}{Re_1}, \frac{1}{Re_2}, \frac{1}{Re_3}\right), \quad (33)$$

Where  $Re_1$ ,  $Re_2$  and  $Re_3$  are the Reynolds numbers for cytoplasm, nucleus and ECM respectively. Here  $s^0 = 0$  and  $v^1, s^1, \phi_b^1, c^1$  are computed by a first order scheme.

For the multiphase field model, the coupled Cahn-Hilliard equations could be solved simultaneously, using preconditioned bicgstab strategy. However, we need to extrapolation the nonlinear terms, which results in a coupled system of the form

$$\partial_t \phi_i + \nabla \cdot (\mathbf{v} \phi_i) = \nabla \cdot (\alpha_{ij} \nabla \phi_j + \beta_{ij} \nabla \nabla^2 \phi_j) + g_i, \quad i = 2, 3.$$

where  $\alpha_j$  and  $\beta_j$  are functions of  $\phi_i$ 's. Thus, the following two equations are solved simultaneously,

$$\frac{3\phi_i^{n+1} - 4\phi_i^n + \phi_i^{n-1}}{2\delta t} + \nabla \cdot (\mathbf{v}^{n+1} \phi_i^{n+1}) = \nabla \cdot (\bar{\alpha}_{ij}^{n+1} \nabla \phi_j^{n+1} + \bar{\beta}_{ij}^{n+1} \nabla \nabla^2 \phi_j^{n+1}) + g_i^{n+1}, \quad i = 2, 3.$$

The numerical scheme is implemented on a graphic processing unit using CUDA. The Nvidia CUFFT, Thrust [13], as well as CUSP [3] have been used to solve the linearized system. The resultant solver is tested in both time and space to ensure it is convergent and attains roughly second order.

## 4 Numerical results and discussion

### 4.1 Parameters and initial setup

For convenience, all parameters used in the model are listed in Table 1 unless noticed otherwise. These parameters are chosen from the published literature or user-defined based on our best guesses. We note that, although we have formulated the three-phase model by treating the nucleus separately as a new phase for eukaryotic cells, this model is also well-suited for studying cytoplasmic dynamics and cytokinesis without considering the nucleus. In those cases, we simply set the initial condition of  $\phi_2$  as zero and assume that  $c_1$  and  $c_2$  are the centers of mass for the cytoplasm distributed on each side of the division plane, respectively. In this two phase model,  $\phi_1$  represents the volume fraction of the substance inside the cell membrane and  $\phi_3$  represents the volume fraction of the buffer, i.e. extra cellular matrix (ECM) outside of the cell membrane.

### 4.2 Dynamics of cell growth and cytokinesis

During the cell mitotic process and before cytokinesis ensues, the parent cell doubles its cytoplasmic volume while in the meantime duplicates its genetic substances (DNAs and chromosomes). The cell morphological change during this process can be studied using the current model by simply shutting down the contracting force and switch on the growth dynamics of the cell, which are characterized by the moments known as the checkpoints present in the current model. At the molecular level, the DNA and chromosome replicate themselves and then separate into two distinct sets of DNAs and chromosomes. Immediately following, two offspring nuclei form, each of which contains the genetic information inherited from the parent cell. This is a complex process involving the formation of mitotic spindle and its elongation in the axis perpendicular to the cytokinetic ring, which is beyond the scope of our current multiphase model's. In the current model, we focus on cytokinesis after the offspring nuclei are separated. We coarse-grain the nucleus as a viscous bulk fluid inside the cytoplasm. After the two offspring nuclei are separated, the nuclei effectively position the division plane, known as the cleavage plane, after which cytokinesis ensues. When the cleavage plane is placed right in the middle of the long axis of the cell, symmetric cell division can be observed. Otherwise, cytokinesis may result in asymmetric division or failure of cytokinesis. We will discuss the case of asymmetric division later, but will not discuss the failure of cytokinesis since its cause is not fully explored yet even experimentally.

In Figure 1, we show a detailed simulation of cytokinesis for eukaryotic cells mentioned above. In particular, the 3D view of the cell growth and division process is portrayed in Figure 1(a-e). The volume of the cytoplasm is doubled at the moment shown in Figure 1(b), after which we see the formation of the cleavage furrow in Figure 1(c), and the abscission that physically cleaves the parent cell into two offspring cells in Figure 1(d). In Figure 1(e), we observe the offspring cell reshapes into round morphology under the influence of surface tension on its own membrane. To our best knowledge, this is the first numerical simulation in full 3D using a hydrodynamic phase field model. To better visualize the dynamics of nucleus in the cytokinesis process, a series of 2D slices at  $x = 0.5$  are plotted in Figure 1(f-j). In particular, the cytoplasmic bridge connecting the two offspring cells is observed (shown in Figure 1(i),) which agrees quantitatively with the morphogenetic pattern obtained from the experimental observations shown in Figure 1(k).

We note that the advantage of the 3D hydrodynamic model is its capability to couple the interior cytoplasmic fluid flow with the exterior fluid flow through the cell membrane and visualize important hydrodynamic quantities such as stress tensors, forces and the hydrostatic pressure throughout the domain during the cellular morphological transformation. In Figure 2, the detail of the viscous stress  $\eta\mathbf{D}$ , volume-averaged velocity  $\mathbf{v}$ , as well as the hydrostatic pressure  $p$  at time  $t = 8.5$  are depicted. The stress tensor at  $(\mathbf{x}, t)$  is visualized as a 3D ellipsoidal object at  $\mathbf{x}$ , whose semiaxes signify the length of the three eigenvalues of the second order symmetric tensor, respectively. From Figure 2(b), a zoomed view of viscous stress tensor is shown. The stress is highly inhomogeneous at the contractile ring on the division plane (cleavage plane), which correlates well with the velocity field shown in Figure 2(f-g), as the cytokinetic ring of the cell is contracting. Besides, the gradient of the hydrostatic pressure is also high at the cleavage plane as well as the interface between the cell nucleus and cytoplasm.

In addition, the distribution of the proxy force and the surface tension force are also shown in Figure 3. Seen from Figure 3(a), the proxy force is mainly distributed on the cell membrane (the interface between cytoplasm and ECM), with much higher values on the division plane, contracting the cell membrane towards the center of the long axis of the cell. This is shown in the 2D view of proxy force in Figure 3(b-c). Same as the proxy force, the surface tension force is also distributed on the interfaces. However, surface tension is more evenly distributed, aiming to smooth out the interface. These two forces oppose to each other on the interface. It is the competition between the surface tension force and the proxy force on the division plane that ultimately contributes to the success of cytokinesis.

### 4.3 Asymmetric Cell Cytokinesis

The positioning of the contractile ring (or cytokinetic ring) located on the division plane is dictated by the mitotic spindle and other intercellular processes. It can affect the morphology of the offspring cells significantly. If the contractile ring is positioned not in a symmetric manner, then asymmetric cell division, or cell polarization could be observed. Asymmetric cell division, which includes cell polarization and cytokinesis is essential for generating cell diversity during development.

Here, we conducted two case studies, where we only concentrate on the cell membrane dynamics by setting  $\phi_2 = 0$ . Note in this case,  $c_1$  and  $c_2$  in the model are chosen as mass

centers of the half cell divided by the cleavage plane. For the first numerical study, we choose the contractile ring on the plane at  $x = 0.9$  with  $L_x = 2.0$  for the whole domain. An asymmetric cell division is simulated shown in Figure 4. The asymmetric cell division in the intermediate stage resembles qualitatively to the budding yeast polarization.

Another case of asymmetric cell division is due to the fact that the concentration of actin-myosin filament is distributed inhomogeneously during cytokinesis. As a simple experiment, we set  $\gamma_{d1}$ , the contractile strength as a function of space, to mimic this inhomogenous contractile force due to the heterogenous distribution of actin-myosin filaments on the division plane. In this context, we set  $\tilde{\gamma}_{d1} = \gamma_{d1}y$ , i.e. the strength of the contractile force is higher on upper membrane of the cell. As a result, a plane-cell type asymmetric cell division can be observed, shown in Figure 5. The cleave furrow is observed in Figure 5(h), which agrees qualitatively with the cleavage in the jellyfish *aequorea*.

## 5 Conclusion

In this paper, we use a multi-phase field model to study cytokinesis of an eukaryotic cell during its mitotic process. Several interesting phenomena such as dynamics and morphological patterns of symmetric or asymmetric cell division in cytokinesis are numerically simulated with the model. These morphological patterns agree qualitatively with experimental observations. This simplified model is thus proven to be an effective tool for studying cytokinesis during the cell division process.

Evidently, this simplified model needs significant improvement in order to make it capable to simulate the complex biological and chemical processes in addition to the mechanical process during the real cell mitotic process. Nevertheless, it marks our first attempt in developing a full 3D hydrodynamic model for cell division in a hydrodynamically consistent way. Within the framework for modeling cell dynamics that the model has provided, we can further superimpose additional features to it or add additional cellular components/structures to it. In our future work, we will incorporate the actomyosin microstructure to the cell cortical layer and derive the contractile force on the cytokinetic ring based on their density and orientational distribution instead of using the proxy force. In addition, the viscoelastic properties of cytoplasm, the chromosome spindle, as well as its elongation on facilitating cytokinesis could be added incrementally as well.

## Acknowledgement

Qi Wang is partially supported by AFOSR, NSF and NIH through awards FA9550-12-1-0178, DMS-1200487, and 2R01GM078994-05A1. Both authors are also partially supported by a SC EPSCOR GEAR award.

## References

- [1] Masakazu Akiyama, Atsushi Tero, and Ryo Kobayashi. A mathematical model of cleavage. *Journal of Theoretical Biology*, 264:84–94, 2010.

- [2] Francis A. Barr and Ulrike Gruneberg. Cytokinesis: placing and making the final cut. *Cell*, 131:847–860, November 2007.
- [3] Nathan Bell and Michael Garland. Cusp: Generic parallel algorithms for sparse matrix and graph computations. *preprint*, 0:0, 2012.
- [4] Gunduz Caginalp and Xinfu Chen. Convergence of the phase field model to its sharp interface limit. *European Journal of Applied Mathematics*, 4:417–445, 1998.
- [5] Julie C. Canman, Lisa A. Cameron, Paul S. Maddox, Aaron Straight, and etc. Determining the position of the cell division plane. *Nature*, 424:1074–1078, August 2003.
- [6] Megan Chircop. Rho gtpases as regulators of mitosis and cytokinesis in mammalian cells. *2014 Special Focus on Rho GTPases*, page e29770, 2014.
- [7] Ulrike S. Eggert, Timothy J. Mitchison, and Christine M. Field. Animal cytokinesis: from parts list to mechanisms. *The Annual Review of Biochemistry*, 75:543–566, 2006.
- [8] Jeffery Errington, Richard A. Daniel, and Dirk-Jan Scheffers. Cytokinesis in bacteria. *Microbiology and Molecular Biology Reviews*, 67(1):52–65, March 2003.
- [9] Michael Glotzer. The molecular requirements for cytokinesis. *Science*, 307:1735–1739, 2005.
- [10] William H. Grover, Andrea K. Bryan, Monica Diez-Silva, Subra Suresh, John M. Higgins, and Scott R. Manalis. Measuring single-cell density. *PNAS*, 108(27):10992–10996, 2011.
- [11] J. L. Guermond, P. Mineev, and Jie Shen. An overview of projection methods for incompressible flows. *Computer Methods in Applied Mechanics and Engineering*, 195:6011–6045, 2006.
- [12] David A. Guertin, Susanne Trautmann, and Dannel McCollum. Cytokinesis in eukaryotes. *Microbiology and Molecular Biology Reviews*, 66(2):155–178, June 2002.
- [13] Jared Hoberock and Nathan Bell. Thrust: a parallel template library. *preprint*, 0:0, 2010.
- [14] Tomasz Kalwarczyk, Natalia Ziebach, Anna Bielejewska, Ewa Zaboklicka, Kaloian Koynov, and etc. Comparative analysis of viscosity of complex liquids and cytoplasm of mammalian cells at the nanoscale. *Nano Letters*, 11(5):2157–2163, 2011.
- [15] Yibao Li, Ana Yun, and Junseok Kim. An immersed boundary method for simulating a single axisymmetric cell growth and division. *Journal of Mathematical Biology*, 65:653–675, 2012.
- [16] Brandon Lindley, Qi Wang, and Tianyu Zhang. A multicomponent model for biofilm-drug interaction. *Discrete and Continuous Dynamical Systems Series B*, 15:417–456, March 2011.

- [17] Brandon Lindley, Qi Wang, and Tianyu Zhang. Multicomponent hydrodynamic model for heterogeneous biofilms: Two-dimensional numerical simulations of growth and interaction with flows. *Physical Review E*, 85:031908, March 2012.
- [18] Ann L. Miller. The contractile ring. *Current Biology*, 21(24):976–978, 2011.
- [19] Nicolas Minc, David Burgess, and Fred Chang. Influence of cell geometry on division-plane positioning. *Cell*, 144:414–426, February 2011.
- [20] Alex Mogilner, Roy Wollman, Gul Civelekoglu-Scholey, and Jonathan M. Scholey. Modeling mitosis. *Trends in Microbiology*, 16(2):88–96, February 2006.
- [21] Krithika Mohan, Pablo A. Iglesias, and Douglas N. Robinson. Separation anxiety: stress tension and cytokinesis. *Experimental Cell Research*, 318:1428–1434, 2012.
- [22] Erich A. Nigg. Mitotic kinases as regulators of cell division and its checkpoints. *Nature Reviews Molecular Cell Biology*, 2:21–32, January 2001.
- [23] Christopher C. Poirier, Win Pin Ng, Douglas N. Robinson, and Pablo A. Iglesias. Deconvolution of the cellular force-generating subsystems that govern cytokinesis furrow ingression. *PLoS Computational Biology*, 8(4), 2012.
- [24] Kathleen E. Rankin and Linda Wordeman. Long astral microtubules uncouple mitotic spindles from the cytokinetic furrow. *The Journal of Cell Biology*, 190(1):35–43, July 2010.
- [25] Elizabeth M. Rechl, Janet C. Effler, and Douglas N. Robinson. The stress and strain of cytokinesis. *Trends in Microbiology*, 15(4):200–206, April 2005.
- [26] Katarzyna A. Rejniak. A single-cell approach in modeling the dynamics of tumor microregions. *Mathematical Biosciences and Engineering*, 2(3):643–655, August 2005.
- [27] Jonathan M. Scholey, Ingrid Brust-Mascher, and Alex Mogilner. Cell division. *Nature*, 422:746–752, April 2003.
- [28] W. Gregory Somers and Robert Saint. A rhogef and rho family gtpase-activating protein complex links the contractile ring to cortical microtubules at the onset of cytokinesis. *Developmental Cell*, 4:29–39, 2003.
- [29] Manuel Thery and Michel Bornens. Cell shape and cell division. *Current Opinion in Cell Biology*, 18:648–657, 2006.
- [30] Paula A. Vasquez and Kerry Bloom. Polymer models of interphase chromosomes. *preprint*, 2014.
- [31] Tianyu Zhang, Nick G. Cogan, and Qi Wang. Phase-field models for biofilms i. theory and simulations. *SIAM Journal of Applied Mathematics*, 69:641–669, 2008.

Table 1: Dimensional Parameters.

Symbol	Description	value	Unit	Reference
T	Absolute Temperature	303	Kelvin	[31]
k	Boltzmann constant	$1.38 \times 10^{-23}$	$m^2 kgs^{-2} K^{-1}$	[31]
$h$	Characteristic length scale	$5 \times 10^{-5}$	m	[23]
$t_0$	Characteristic time scale	0.1	s	[23]
$\rho$	Reference density	$1.1 \times 10^3$	$kgm^{-3}$	[10]
$\eta_1$	Dynamic viscosity of cytoplasm	$1 \times 10^{-2}$	$kgm^{-1}s^{-1}$	[14]
$\eta_2$	Dynamics viscosity of nueclues	$2 \times 10^{-2}$	$kgm^{-1}s^{-1}$	
$\eta_3$	Dynamics viscosity of ECM	$5 \times 10^{-3}$	$kgm^{-1}s^{-1}$	[14]
$\gamma_{A,B,C}$	Distortional energy coefficient	$2.5 \times 10^7$	$m^{-1}$	
$\gamma_{1,2,3}$	Bulk free energy coefficient	$1.875 \times 10^{20}$	$m^{-3}$	
$\gamma_{123}$	Lagrangian multiplier strength	1.0	$m^{-3}$	
$\lambda_{1,2,3}$	Motility parameter for each component	$1 \times 10^{-11}$	$kg^{-1}m^3s$	
$c_1$	Growth rate of cytoplasm	5.0	$s^{-1}$	
$c_2$	Growth rate for nucleus	5.0	$s^{-1}$	
$\gamma_{d1}$	Stimulating force strength	2.5	$m^{-3}$	
$\gamma_{d2}$	Stimulating force strength	15	$m^{-3}$	
$\varepsilon_d$		0.01		



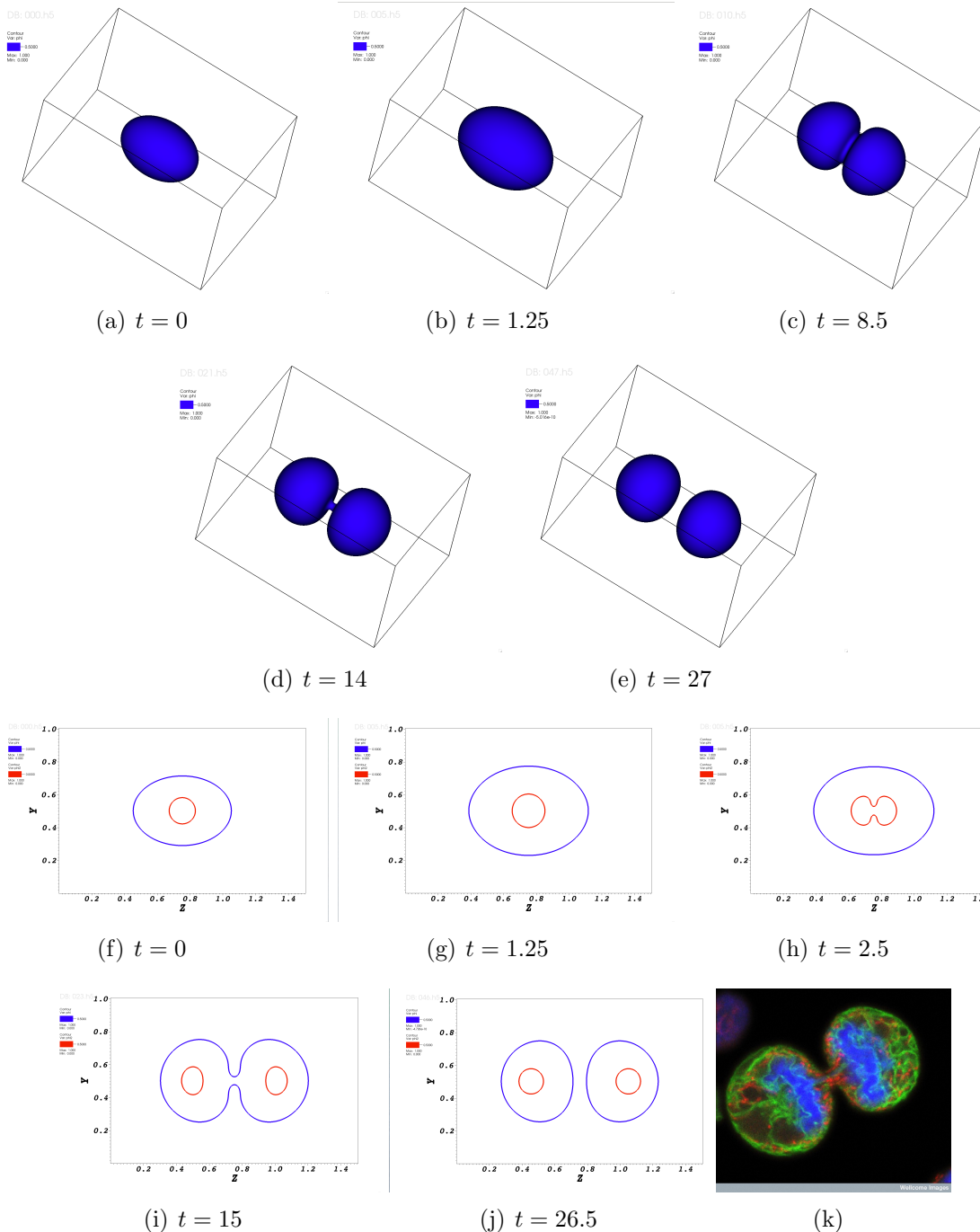


Figure 1: Cell growth and cytokinesis. This figure shows a parent cell duplicates its nucleus and cytoplasm, then splits into two identical offspring cells. (a)-(e) 3D Numerical simulations of the cell division process at different stages; (f-j) 2D slices at  $x = 0.5$  for the cell division process; (k) a dividing melanoma cell just before it divides into two offspring cells completely. **Permission is needed from, [http : //php.med.unsw.edu.au/cellbiology/index.php?title = File : Melanoma<sub>c</sub>ytokinesis.jpg](http://php.med.unsw.edu.au/cellbiology/index.php?title=File:Melanoma_cytokinesis.jpg).**

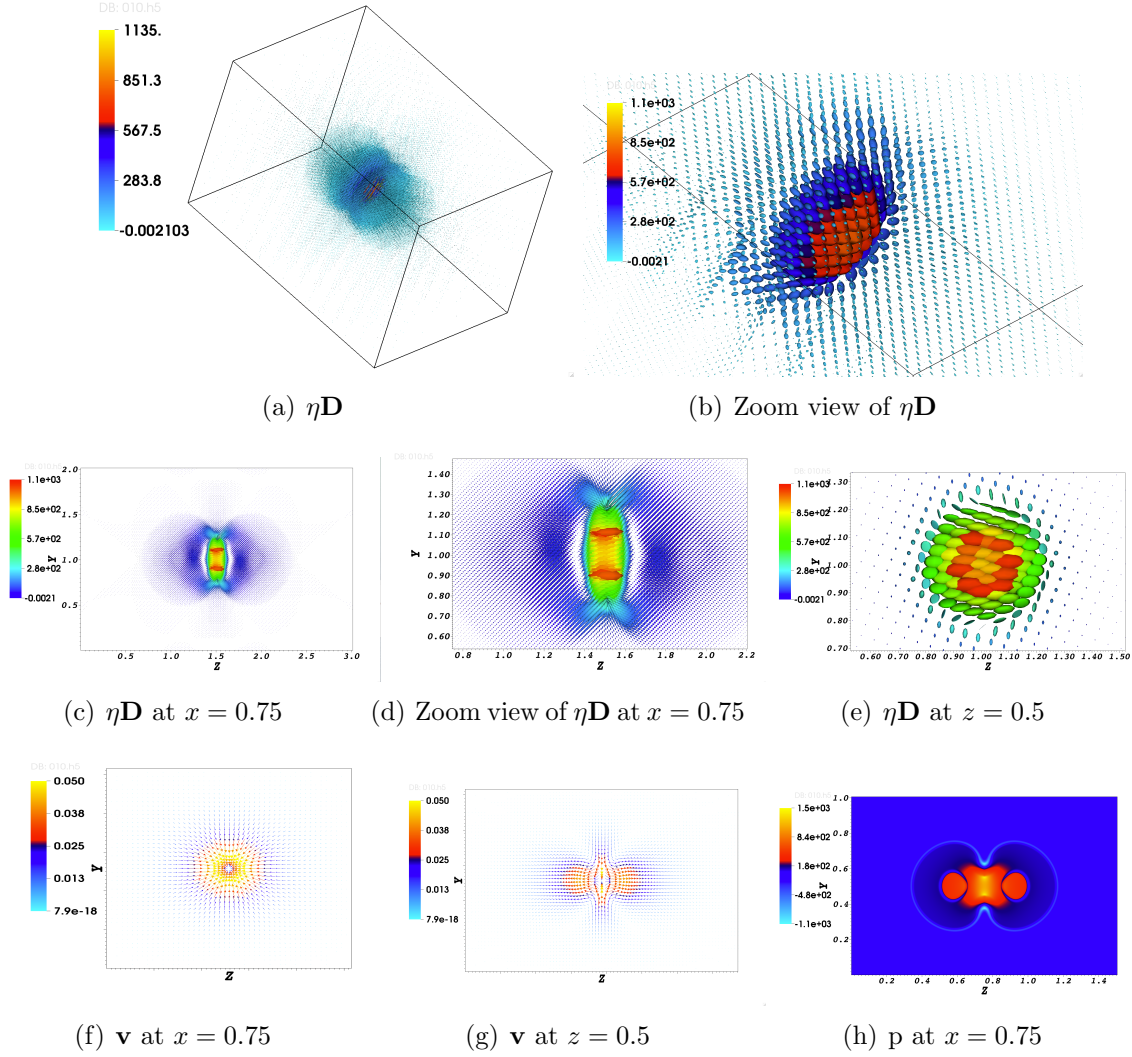


Figure 2: Hydrodynamic variables at  $t = 8.5$ . This figure shows the hydrodynamic variables, including viscous stress tensor  $\beta\mathbf{D}$ , volume-averaged velocity  $\mathbf{v}$  and the hydrostatic pressure  $p$  distribution at time  $t = 8.5$  for the simulation shown in Figure 1. (a) 3D view of the stress tensor as ellipsoids; (b) a zoomed view of the stress tensor; (c-e) 2D slices of the stress tensor field; (f-g) 2D slices of the velocity field; (h) a 2D slice of the pressure field.

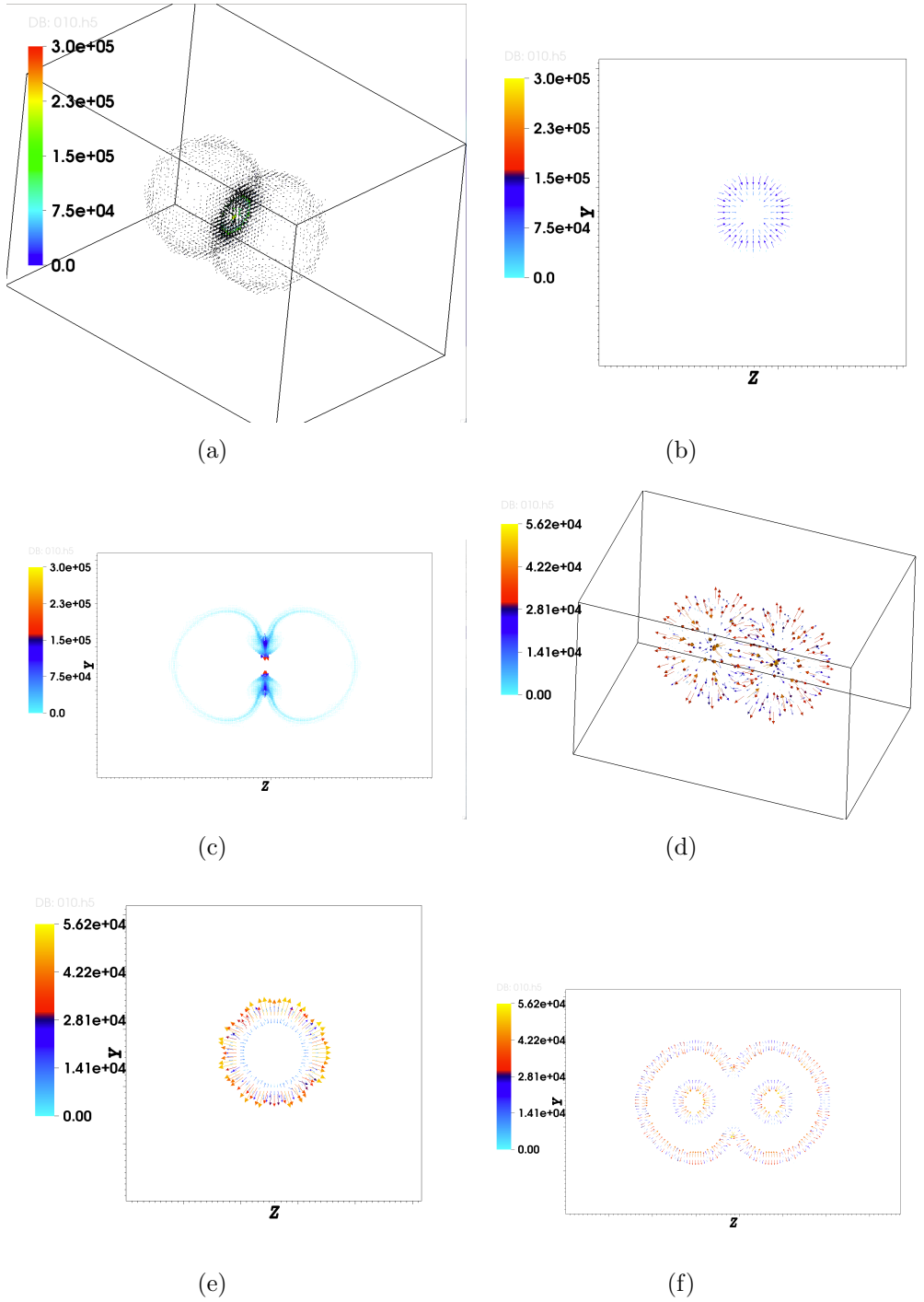


Figure 3: Visualization of the proxy force and the surface tension force. This figure shows the proxy force and surface tension force at time  $t = 8.5$  of the simulation shown in Figure 1. (a) 3D view of the proxy force; (b) a 2D slice of proxy force at  $x = 0.5$ ; (c) a 2D slice of proxy force at  $z = 0.5$ ; (d) 3D view of the surface tension force; (e) a 2D slice of the surface tension force at  $x = 0.5$ ; (f) a 2D slice of the surface tension force at  $z = 0.5$ . The proxy force opposes to the surface tension force at the cytokinetic ring.

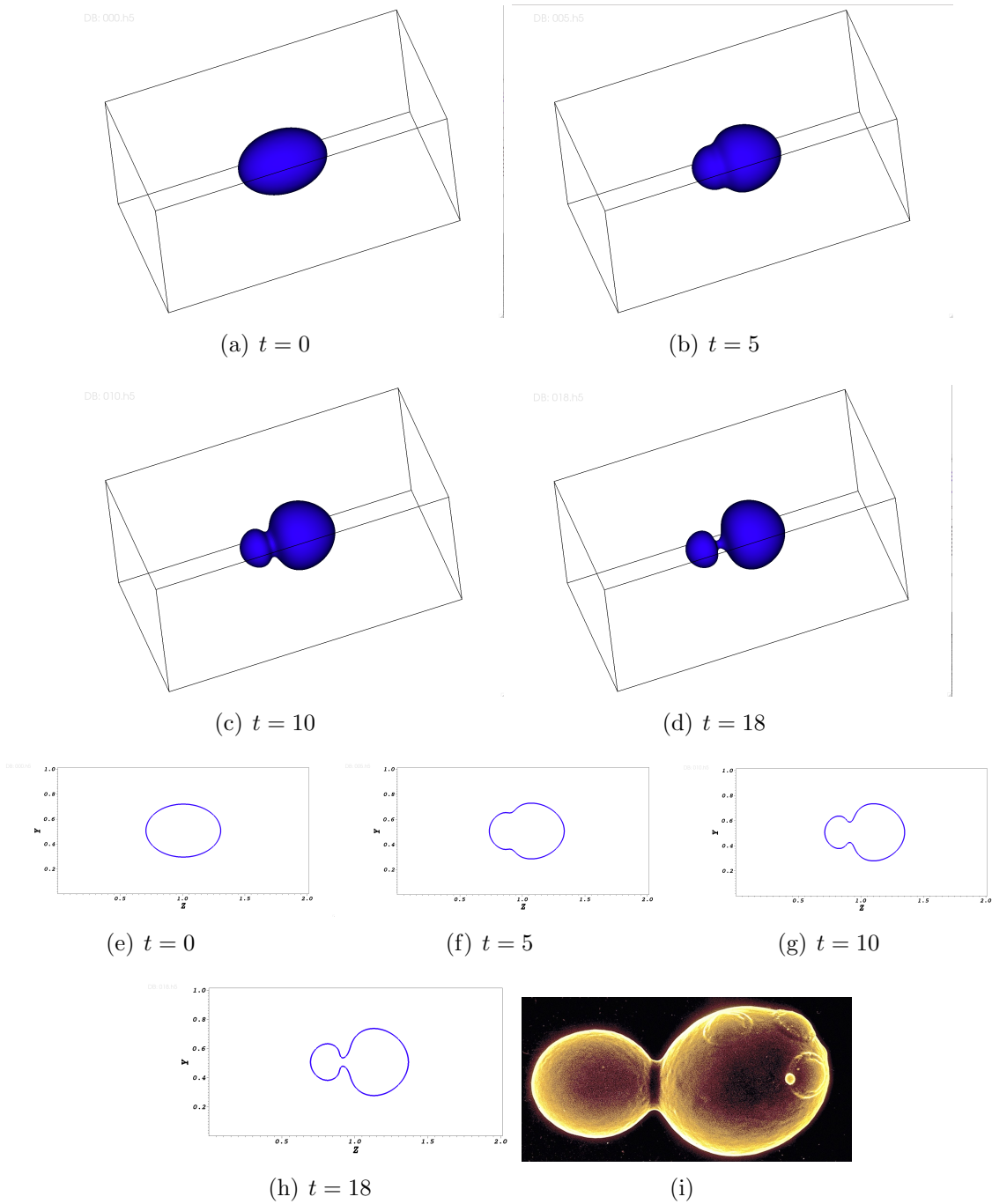


Figure 4: Asymmetric cell division due to the asymmetric positioning of cleavage plane. This figure shows an asymmetric cell cytokinesis process in which the division plane is positioned in an asymmetric fashion along the long axis of the cell. (a)-(d) 3D Numerically simulated cell division process at different time; (e-h) 2D slices ( $z = 0.5$ ) of cell division process at different time; (f) a budding yeast. This asymmetric cell division resembles the yeast cell budding process. **A permission is needed from <http://www.ppdictionary.com/fungi.htm>**

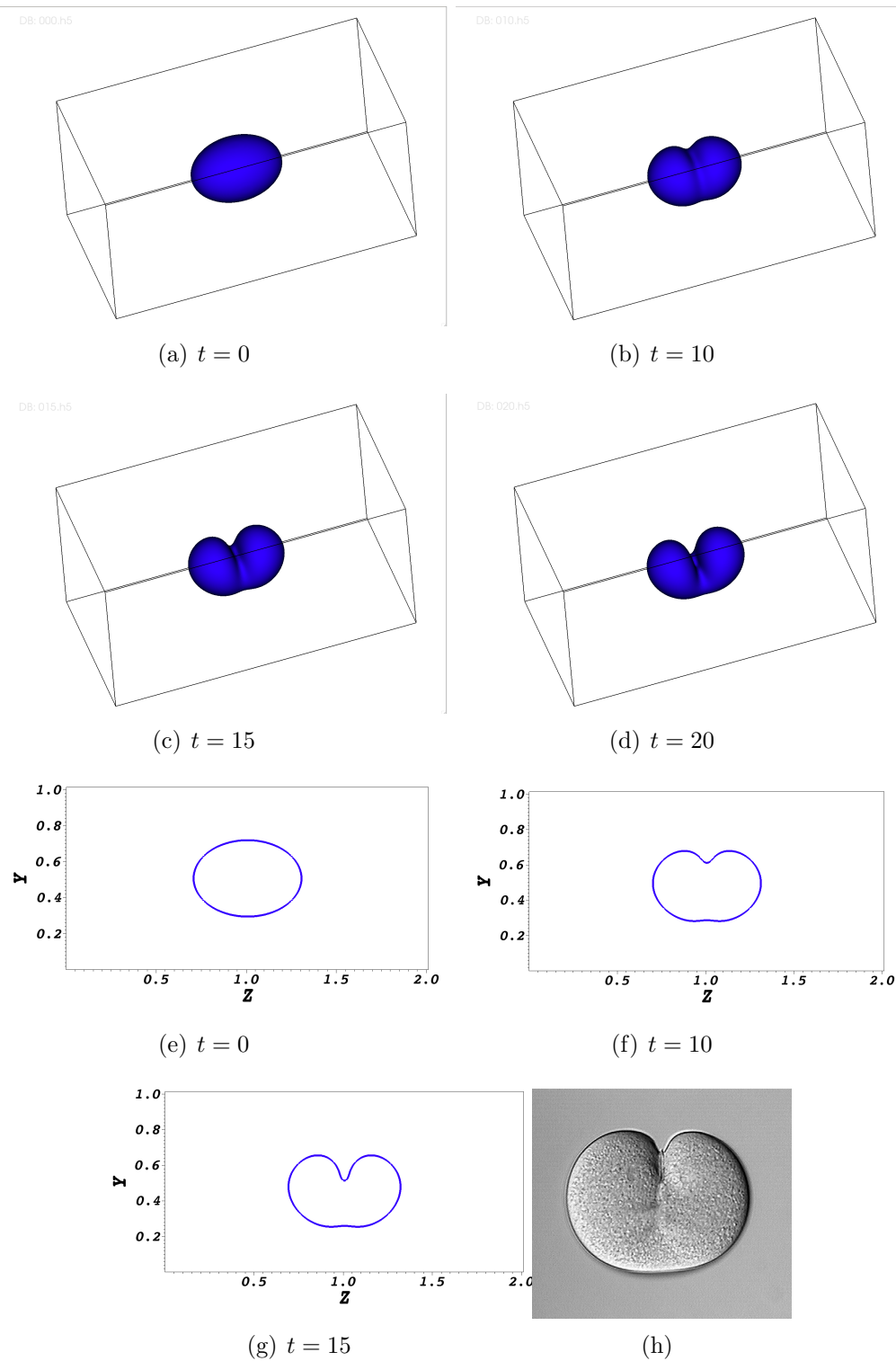


Figure 5: Asymmetric cleavage furrow formation due to inhomogeneous actomyosin distribution. This figure shows the asymmetric cleavage furrow formation due to the inhomogeneous contractile force along the cytokinetic ring induced by heterogeneous actomyosin distribution on the contractile plane. (a-d) 3D view of the asymmetric cell division at different time; (e-g) 2D slices ( $z = 0.5$ ) of the asymmetric cell division at different time; (h) cleavage furrow in the jellyfish *Aequorea*. **A permission is needed from <http://celldynamics.org/embryos/aequorea20.html>.**